Attenuation correction of SPECT images based on separately performed CT

Effect on the measurement of regional uptake values

Schwächungskorrektur von SPECT mit separaten CT-Daten: Effekte auf die regionale Traceranreicherung

W. Römer[1], E. Fiedler[1], M. Pavel[2], A. Pfahlberg[3], T. Hothorn[3], H. Herzog[4], W. Bautz[5], T. Kuwert[1]
Clinic of [1]Nuclear Medicine (Prof. Dr. T. Kuwert), [2]Internal Medicine I (Prof. Dr. E. G. Hahn), [3]Department of Medical Informatics, Biometry and Epidemiology (Prof. Dr. O. Gefeller), [5]Institute of Diagnostic Radiology (Prof. Dr. W. Bautz), University of Erlangen/Nürnberg, Erlangen, Germany
[4]Institute of Medicine (Prof. Dr. K. Zilles), Forschungszentrum Jülich GmbH, Jülich, Germany

Keywords
SPECT, attenuation correction, image fusion, spiral computed tomography, indium-111-pentetreotide

Summary
Aim: A new software approach uses separately acquired CT images for attenuation correction after retrospective fusion with the SPECT data. This study evaluates the effect of this CT-based attenuation correction on indium-111-pentetreotide-SPECT images. Methods: Indium-111-pentetreotide-SPECT imaging using a dual-head gamma camera e.cam (Siemens Medical Solutions, Erlangen, Germany) as well as separate spiral computed tomography (CT) was performed in 13 patients. After fusion of SPECT and CT data, the bilinear attenuation coefficients were calculated for each pixel in the CT image volume using their Hounsfield unit values and attenuation-corrected images were reconstructed iteratively (OSEM 2D). Regions of interest (ROIs) were drawn on 24 suspicious foci and background, and target to background ratios were calculated for corrected (TBAC) and uncorrected (TBNAC) images. The shortest distance from the centre of the lesion to the surface of the body (DS) was measured on the corresponding CT slice. Furthermore, ROIs were drawn over the rim and the centre of the liver. Ratios of hepatic count rates for corrected (LRAC) and uncorrected (LRNAC) images were also compared. Results: In lesions located more centrally, TBAC was up to 52% higher, whereas in peripherally located lesions, TBAC was up to 63% lower than TBNAC. The TBAC/TBNAC quotient was linearly correlated with DS. In the liver, attenuation correction resulted in a 35% increase of LRAC compared with LRNAC. Conclusions: Attenuation correction of SPECT images performed by separately acquired CT data is quick and simple. It improves the contrast between target and background for lesions located more centrally in the body and improves homogeneity of the visualisation of tracer uptake in the liver.

Nuklearmedizin 2005; 44: 20–8

Schlüsselwörter
SPECT, Schwächungskorrektur, Bildfusion, Spiral-CT, Indium-111-Pentetreotide

Zusammenfassung
Ziel: Mit Hilfe einer neuen Software können SPECT-Bilder nach Fusion mit separat aufgenommenen CT-Bildern schwächungskorrigiert werden. Wir untersuchten den Effekt dieser CT-basierten Schwächungskorrektur auf Indium-111-Pentetreotid-SPECT-Bilder. Methoden: 13 Patienten mit neuroendokrinen Tumoren erhielten ein Indium-111-Pentetreotid-SPECT unter Verwendung einer Doppelkopf-SPECT-Kamera e.cam (Siemens Medical Solutions, Erlangen, Germany) sowie zeitlich davon getrennt ein Spiral-CT. Nach Fusion der SPECT- und CT-Bilder wurden pixelweise bilinear Schwächungskoeffizienten anhand der Hounsfield-Werte aus den CT-Daten errechnet und schwächungskorrigierte Bilder mittels iterativer Rekonstruktion erzeugt (OSEM 2D). Über fokalen Mehranreicherungen (n = 24) und über dem Hintergrund wurden ROIs (regions of interest) gezeichnet und Target/Hintergrund-Quotienten für die schwächungskorrigierten (TBAC) und nicht schwächungskorrigierten (TBNAC) Datensätze ermittelt. Auf den korrespondierenden CT-Schichten wurde der minimale Abstand des Zentrums der Läsion von der Körperoberfläche (DS) gemessen. Außerdem wurde je eine ROI über der Leberperipherie und der Lebermitte positioniert und die Countratenverhältnisse mit (LRAC) und ohne (LRNAC) Schwächungskorrektur verglichen. Ergebnisse: TBAC war bei mehr zentralen Herden bis zu 52% höher, bei peripheren Läsionen dagegen bis zu 63% niedriger als TBNAC. Der Target/Hintergrund-Quotient zeigt eine lineare Korrelation mit DS. In der Leber führte die Schwächungskorrektur zu einem Anstieg von LRAC um 35% verglichen mit LRNAC. Schlussfolgerung: Die Schwächungskorrektur von SPECT-Bildern mit separaten CT-Daten ist schnell und einfach. Der Kontrast zwischen zentralen Läsionen und dem Hintergrund wird verbessert, die Traceraufnahme in der Leber kommt homogener zur Darstellung.

Single photon emission computed tomography (SPECT) is frequently used in nuclear medicine to improve diagnostic accuracy. However, it is well known that attenuation effects cause artefacts in SPECT images (5, 24). Due to these artefacts, and depending on the location of lesions, the target to background contrast will vary. In addition, the absolute quantitation of tracer uptake in SPECT is hampered by attenuation effects and detection of scattered radiation.

The goal of the processing of SPECT images is to supply physicians with accurate and reliable images, leading to correct medical diagnoses. Correcting for the deterioration of the data acquired caused by attenuation can potentially contribute to this goal. Up to now, in particular in nuclear cardiology, several approaches to achieve attenuation correction were attempted (17). In order to perform attenuation correction, a map of regional attenuation coefficients has to be generated. These are determined either based on a user defined contour, by transmission scanning using point or line-sources integrated into the gamma camera or by a computed tomographic (CT) system attached to the gamma camera (7, 16). The latter also allows for exact anatomic localisation of SPECT lesions. Currently, only one commercial in-line SPECT/CT device is available, which uses a continuously rotating x-ray CT tube and detector attached to the same rotating gantry to which the gamma camera heads are mounted (11). However, rotation speed as well as tube current is limited and image quality is degraded as compared with routine spiral

Received: March 3, 2004; in revised form: September 8, 2004

Tab. 1 Clinical and demographic data of the patients

Patient no.	Age (years)	Interval SPECT-CT (days)	Duration of fusion (seconds)	LRAC/ LRNAC	Tumour type	Lesion location	Number of lesions
1	44	5	68	1.39	Metastatic NET	-	-
2	79	1	65	1.27	NET, duodenum	Para-aortic	1
3	55	1	143	1.34	Metastatic NET	Para-aortic	1
4	68	15	65	-	Medullary thyroid carcinoma	Axilla	2
5	74	6	77	1.55	Metastatic NET	Lung	2
			52			Liver	1
						Para-aortic	2
6	65	5	110	1.16	Metastatic NET	Liver	4
						Para-aortic	2
7	64	27	62	1.23	Suspected NET, pancreas	Breast	1
						Axilla	1
8	64	5	75	1.34	Metastatic NET	Para-aortic	1
9	38	3	64	1.34	Carcinoid, ileum	Mesenteric	2
10	73	0	85	1.34	Metastatic NET	Liver	3
11	43	2	52	1.35	Suspected insulinoma	-	-
12	56	3	62	1.53	Gastrinoma	Stomach	1
13	61	1	90	1.40	Carcinoid, transverse colon	-	-

NET, neuroendocrine tumour

CT scanning. This is in contrast to current hybrid systems combining positron emission tomography (PET) and high-end spiral CT scanners (21).

In this publication, we report results obtained by a new software approach, which performs attenuation correction of SPECT images using separately acquired CT data. Firstly, CT and reconstructed SPECT images are manually registered. Following this, an attenuation map is calculated from the CT data and used for the attenuation correction of the SPECT data.

The aim of the study presented here was to evaluate the effect of attenuation correction on the target to background contrast in correlation with the location of lesions. Furthermore, we sought to determine the time expense for generating attenuation-corrected data. In addition, the homogeneity of tracer uptake in the liver was analysed before and after attenuation correction. SPECT imaging was performed using the somatostatin analogue indium-111 pentetreotide in patients suffering from neuroendocrine tumours. For further validation of the results obtained with the patients, phantom studies were also performed.

Patients, material and methods

Patients

Thirteen patients (3 men, 10 women; age range: 38-79 years, mean 60 years) consecutively examined with indium-111 pentetreotide scintigraphy were included in this study. The patients' demographic and clinical data are given in Table 1.

CT scanning

In all patients, CT scans from the upper thorax to the groin were obtained before indium-111 pentetreotide scintigraphy. The average time interval between CT and SPECT was 5 days, ranging from 0 to 27 days. Either a 16-slice CT-scanner (SOMATOM Sensation 16) or a 10-slice CT-scanner (SOMATOM Sensation 10) was used. The CT scans were performed according to routine protocols in maximum inspiration using intravenous contrast agent as well as oral contrast material for abdominal scanning. The scan parameters for the CT from the upper thorax to the groin were: 120 kV; 160 mAs; rotation time 0.5 seconds; collimation 16 x (resp. 10 x) 0.75 mm. The scans were performed in a supine position with elevated arms in breath-hold inspiration. Image reconstruction resulted in images with a slice width of 5 mm using a 5 mm reconstruction increment.

Somatostatin receptor scintigraphy and SPECT

For somatostatin receptor scintigraphy, on the average 187 MBq (141-251 MBq) indium-111 pentetreotide (OctreoScan, Mallinckrodt, St. Louis, USA) was injected intravenously. Whole-body scintigraphy was performed 4 h and 24 h after injection. In addition, SPECT was obtained 24 h after injection over the anatomical regions showing pathological tracer uptake. For this purpose, the dual-head gamma camera e.cam (Siemens Medical Solutions, Erlangen, Germany), fitted with medium-energy collimators and interfaced with an e.soft acquisition station (Siemens Medical Solutions, Erlangen, Germany), was used. Counts from the 20% energy windows at 172 keV and 247 keV were acquired into a 64×64 matrix (pixel size 9.3×9.3 mm). A total of 30 views, each of a duration of 60 s, was acquired over 360°.

Data reconstruction

SPECT and CT data were transferred to the e.soft processing workstation. Raw SPECT data were reconstructed into transaxial slices using the e.soft reconstruction software. Reconstruction was performed iteratively by using the ordered subsets expectation maximization (OSEM 2D) technique with 8 iterations and 4 subsets. Images were smoothed with a 3D spatial Gaussian filter (FWHM 18 mm).

Afterwards, SPECT and CT data were fused using the Syngo 3D advanced image fusion tool (Siemens Medical Solutions, Erlangen, Germany) and then implemented into the e.soft software for further processing. The fusion of both data sets was done manually using intrinsic body markers such

as the contours of the body, of the liver, and of organs exhibiting intensive tracer uptake such as the spleen, the kidneys, or tumour lesions (Fig. 1). Image fusion was performed by a physician trained both in CT as well as in SPECT who did not know these image sets and its duration was recorded. The process of fusion resulted in co-registered data that were used for the calculation of the attenuation map. Afterwards, the bilinear attenuation coefficient for each pixel in the CT image volume downscaled from a 512 × 512 matrix to 64 × 64 was calculated, based on its Hounsfield unit value (Fig. 1).

In the CT scans, the contrast material was distributed homogenously within the parenchymal structures and the Hounsfield units did not differ significantly from values given in literature (8). Therefore, intravenous as well as oral contrast material was of minor influence on calculating the attenuation coefficient. For the multiple energy isotope indium-111, where data have been collected from two peaks (172 keV and 247 keV) and summed into one acquisition window, an effective energy of 207 keV which corresponds to the branching ratio averaged energy of the emission energies was entered manually.

Attenuation correction was automated using the workflow implemented in the e.soft software (attenuation map activity) and its duration was measured as well. The attenuation correction method used in our study includes the attenuation in the forward as well as backward projections of the implemented OSEM 2D reconstruction. Therefore, this bilinear attenuation correction is not a multiplicative correction. Scatter correction was indirectly considered by utilizing a broad beam model in the reconstruction, where attenuation values are reduced by some factor compared to the theoretical ones. Generally, this factor depends on the energy of the tracer and the acquisition window width. In our studies, the default factor for indium-111 as given by the manufacturer was 0.8529.

The attenuation-corrected data were reconstructed identically as were the non corrected data. Both data sets were displayed in the transaxial, coronal, and sagittal planes.

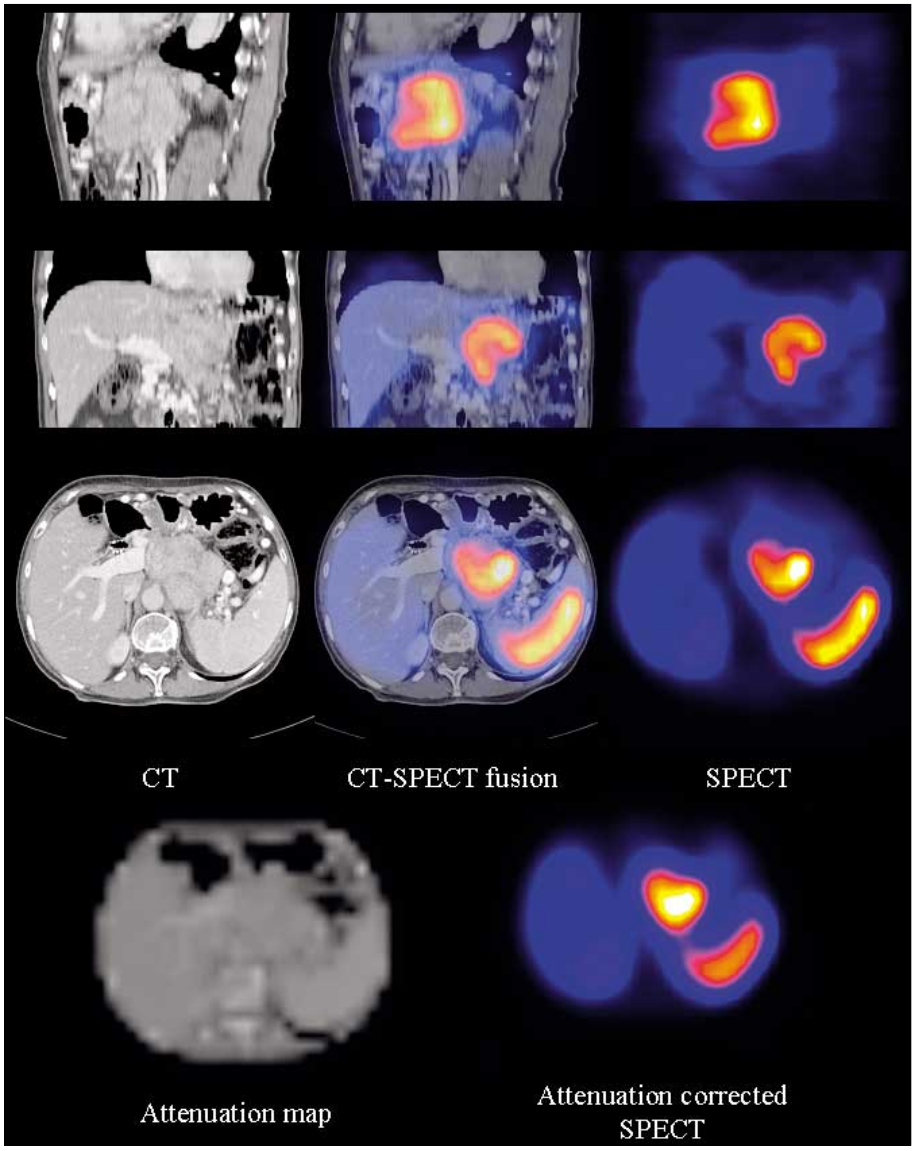

Fig. 1 Metastatic lesion of a neuroendocrine tumour located in front of the aorta just below the pancreatic tail. Corresponding transaxial slices from CT and reconstructed indium-111 pentetreotide SPECT as well as fusion image, attenuation map, which represents the attenuation coefficients for each pixel in a 64 x 64 matrix, and resulting attenuation corrected SPECT image are shown. SPECT images are calibrated to their own maxima, white is indicating the highest values. Note increases in uptake values in the metastatic lesion on the attenuation-corrected image.

Data analysis

Reconstructed transaxial slices were visually analysed on the monitor screen to detect foci of pathological tracer uptake. The attenuation-corrected transaxial image through the maximum of tracer uptake in the tumour lesion was selected for further analysis. A total of 24 suspicious foci were detected. On each focus, an irregular region of interest (ROI) with a mean size of 14 pixels (range 5-46 pixels) was manually drawn. A background ROI over the perifocal area of roughly 50 pixels was defined in a ring-like shape excluding areas of increased tracer uptake in the neighbourhood of the focus. In addition, a further background ROI of roughly 50 pixels was drawn over the vertebral area. The presence of bone metastases in this area was excluded by visual analysis. Formerly, it has been shown in gliomas that maximal uptake values yielded the highest levels of significance in group comparisons of tumour

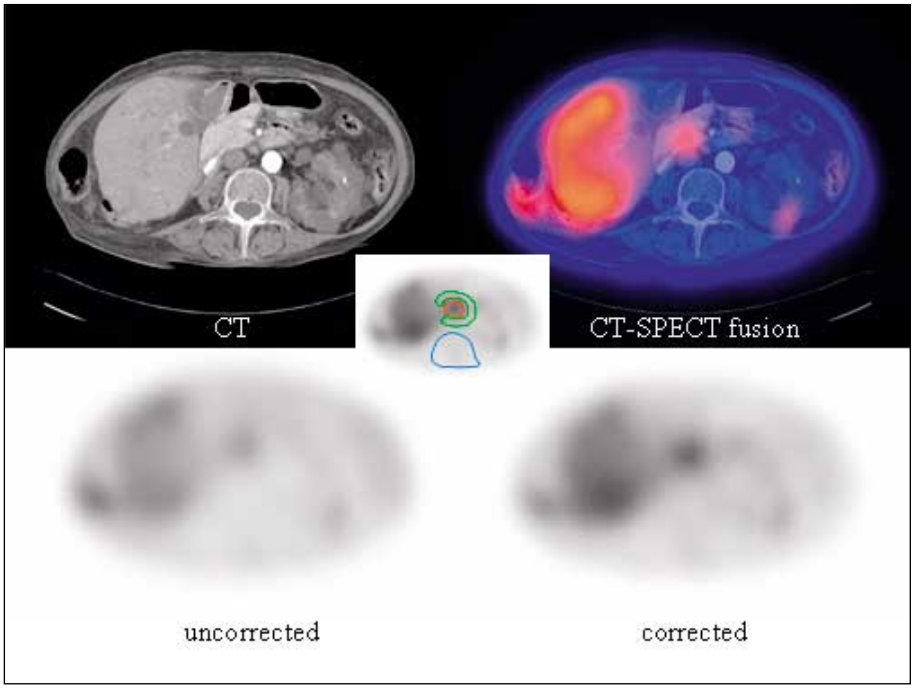

Fig. 2 Neuroendocrine tumour of pancreatic head. Corresponding transaxial slices from CT, CT/indium-111-pentetreotide-SPECT fusion as well as SPECT without and with attenuation correction are shown. The tumour was not visible on the CT scan. However, biopsy during endoscopy confirmed its presence at that location. SPECT images are calibrated to their own maxima. The intensity in the centre of the image increased after attenuation correction, meanwhile the structures located at the periphery remained equal. In this case, TBAC/TBNAC$_{vertebral}$ is 1.52. On the picture inserted in the centre, the ROI over the focus, the perifocal ROI and the vertebral ROI are shown.

Patient no.	Lesion location	Distance from body surface (mm)	TBAC/TBNAC perifocal	TBAC/TBNAC vertebral
2	Para-aortic	97	1.18	1.52
3	Para-aortic	94	1.13	1.49
4	Axilla	42	1.07	0.95
	Axilla	33	1.05	0.86
5	Lung	37	0.80	0.52
	Lung	50	0.97	0.37
	Liver	61	0.79	0.47
	Liver	24	0.76	1.02
	Para-aortic	76	0.99	0.92
6	Liver	32	0.78	0.88
	Liver	31	0.72	0.48
	Liver	38	0.79	0.56
	Liver	64	1.07	1.25
	Para-aortic	127	1.20	1.32
	Para-aortic	129	1.11	1.14
7	Breast	22	0.59	0.49
	Axilla	35	0.81	0.76
8	Para-aortic	94	1.19	1.29
9	Mesenteric	78	1.04	1.07
	Mesenteric	70	1.07	0.98
10	Liver	63	0.87	0.79
	Liver	63	0.82	0.77
	Liver	31	1.14	0.73
12	Stomach	102	0.93	0.98

Tab. 2 Lesion location, distance from the surface of the body, and relative indium-111 pentetreotide uptake values in the lesions

uptake in SPECT imaging using the amino acid ^{123}I-α-methyl tyrosine (15). Therefore, we used maximal uptake values measured in the tumours for further analysis.

For the background ROIs, average counts per ROI were determined. For further analysis, ratios between maximal tracer uptake in the neoplastic lesion on the one hand and average tracer uptake in the two background ROIs (TBAC$_{perifocal}$ and TBAC$_{vertebral}$, resp.) were calculated in order to evaluate lesion contrast.

ROIs were then copied to identical positions in the corresponding non-corrected slice and count rates were calculated in the same way (TBNAC). Changes in lesion contrast were quantified by dividing relative count rates determined with and without attenuation correction (TBAC/TBNAC).

The minimal distance between the centre of the lesion to the surface of the body (DS) was measured by the calliper implemented in the Syngo viewing software (Siemens Medical Solutions, Erlangen, Germany) on the corresponding CT slice.

In addition, circular ROIs (10 pixels, 920 mm^2) were manually drawn over the lateral rim and the centre of the liver. Count rate ratios for corrected (LRAC) and uncorrected (LRNAC) images were compared. Linear ROIs were drawn on selected slices with and without attenuation correction and line profiles were displayed.

Phantom study

A phantom study was performed to examine the primary efficiency of the AC by testing if the AC yields a flat horizontal profile crossing the reconstructed image of a ho-

mogeneously filled phantom. For this purpose, a cylindrical phantom filled with water was scanned with a 10-slice CT-scanner (SOMATOM Sensation 10) using identical scanning and reconstruction parameters as indicated above. Afterwards, the phantom was filled with water containing 0.8 MBq/l of indium-111 and SPECT was obtained under the same conditions as in patients. Data reconstruction was performed in an identical manner resulting in uncorrected and corrected slices. Linear ROIs were drawn on selected slices with and without attenuation correction and line profiles were displayed.

Statistical analysis

Differences in uptake ratios were tested using the sign test. The Spearman correlation coefficient was calculated to analyse the correlation of relative uptake values with focus depth. A linear regression analysis was performed to analyse the correlation of TBAC/TBNAC with the distance of the lesion to the surface of the body. The count rates in the ROIs over the rim and the centre of the liver were compared using the sign test in data with and without attenuation correction. Results with p-values less than 5% were considered significant.

Results

The manual alignment of CT and SPECT data judged as optimal by visual criteria was completed on average in 76 seconds (range 52-143). The automatic process of attenuation calculation and the attenuation weighted reconstruction took less than 2 minutes in all studies.

Figures 1 and 2 give representative images. 24 suspicious foci were detected. Table 2 lists the corresponding values of tracer uptake. In addition, for each lesion the location and the distance from the surface of the body are given. No significant relationship between relative uptake values and the distance of the lesions to the surface of the body could be demonstrated (Spearman correlation coefficient = 0.27; p >0.05).

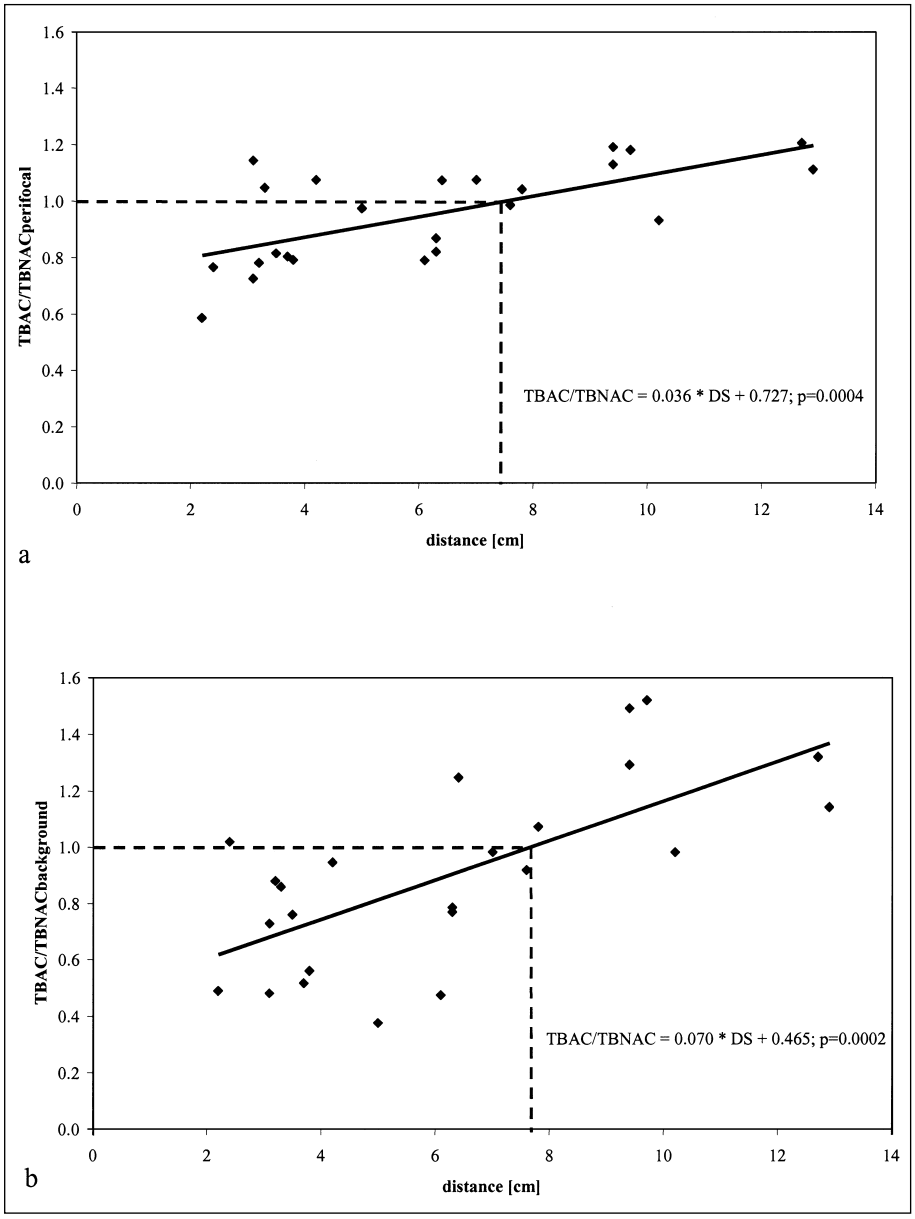

Fig. 3 $TBAC/TBNAC_{perifocal}$ (a) and $TBAC/TBNAC_{vertebral}$ (b) plotted against the minimal distance of the lesions from the surface of the body. The dotted line indicates the distance for which the lesion contrast in attenuation-corrected and uncorrected images is equal.

Also, the introduction of the ROI size into the analysis as a covariate had no significant effect.

Target to background contrast

In lesions located closer to the centre of the body, TBAC was up to 52 % higher (Fig. 2). In peripherally located lesions, TBAC was up to 63 % lower than TBNAC. The TBAC/TBNAC quotient was significantly correlated with the distance of the lesion from the surface of the body (Fig. 3). This correlation was linear:

$TBAC/TBNAC_{perifocal}$ =
0.036 * DS + 0.727 (p = 0.0004).

The formula indicates that TBAC increases by 4% as compared to TBNAC when the distance from the surface of the body in-

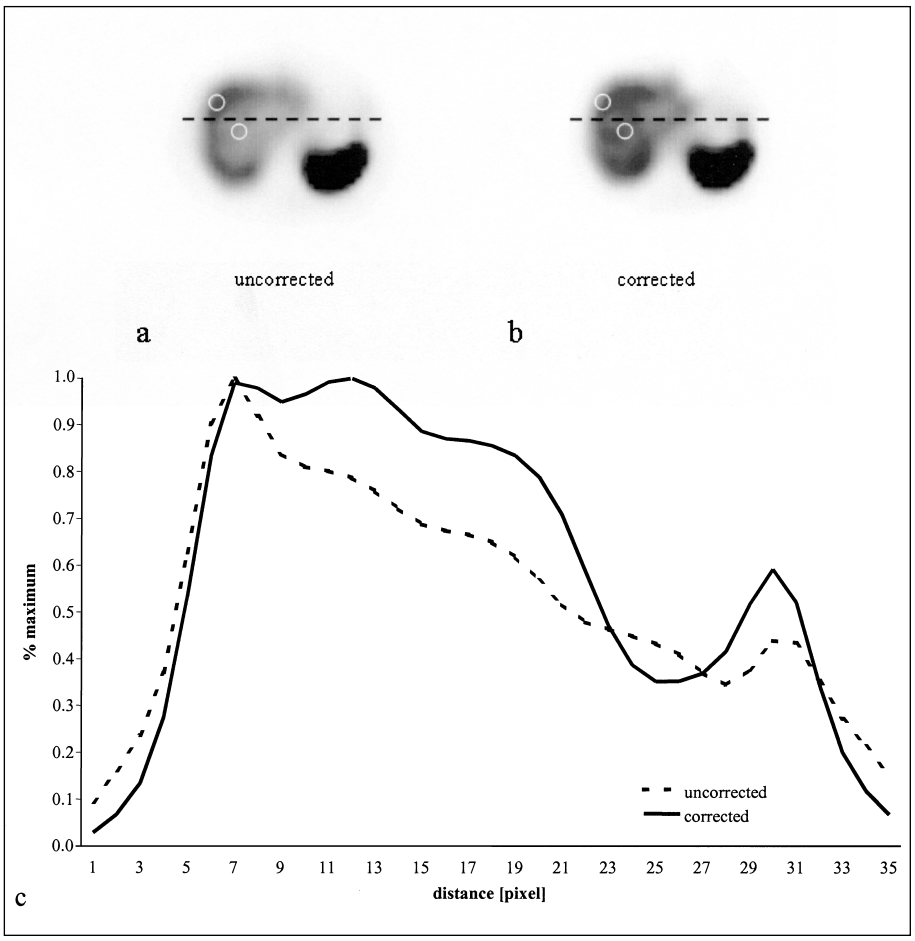

Fig. 4 Transaxial slices from indium-111 pentetreotide SPECT without (a) and with (b) attenuation correction: Images show improved homogeneity of tracer uptake in the liver after attenuation correction. The circular ROIs are representative for the region used to calculate the count rate ratios between the lateral rim and the centre of the liver for corrected (LRAC) and uncorrected (LRNAC) images. In the case displayed, LRAC/LRNAC was 1.34. Curves (c) represent line profiles from right to left comparing attenuation-corrected and uncorrected slices.

creases by 1 cm. The distance from the surface of the body for which the target to background contrast was equal in attenuation-corrected and uncorrected images was approximately 8 cm.

Liver homogeneity

In images not corrected for attenuation, the count rates of the ROIs drawn over the lateral rim of the liver were significantly different from the count rates of the ROIs drawn over the centre of the liver (664 ± 395 vs. 544 ± 318; p = 0.006). In contrast, with attenuation correction, no statistically significant difference was found for these variables (2365 ± 1707 vs. 2514 ± 1475; p = 0.146). Attenuation correction resulted in a 35% increase (range 16-55) of LRAC compared with LRNAC. In Figure 4, in addition to attenuation-corrected and uncorrected slices, a line profile through the upper abdomen is displayed. The curves show the increase in homogeneity of tracer uptake in the liver on the attenuation-corrected image as compared to the uncorrected image.

Phantom data

The outcome of the phantom measurement as shown in Figure 5 demonstrates the efficiency of the CT-derived attenuation correction applied here. In contrast to the image without AC a homogenous tracer distribution is reconstructed when including the attenuation correction. This visual impression is confirmed by the horizontal profile crossing the homogeneously filled cylindrical phantom.

Discussion

To all our knowledge, this is the first clinical evaluation of a new commercially available software for attenuation correction of SPECT based on separately acquired CT data. In order to enable attenuation correction of the SPECT data, image registration is performed by visual alignment of the SPECT and CT images using internal landmarks such as the contours of the body, of the liver and of organs exhibiting intensive tracer uptake such as the spleen, the kidneys, or neoplastic lesions. No external markers are used. The Hounsfield numbers of the CT images are converted to attenuation coefficients corresponding to the photon energy of the respective nuclide, thus generating an attenuation map, which is utilized in the attenuation weighted OSEM-2D reconstruction (22, 23).

The approach to convert the Hounsfield numbers into the attenuation coefficients valid for indium-111 was supplied by the manufacturer of our SPECT system. The horizontal profile crossing the reconstructed image of a homogeneously filled cylindrical phantom demonstrates that the attenuation correction with its implicit scatter compensation works sufficiently.

In our study the whole process including manual image fusion and automated attenuation correction was performed in less than four minutes. Data on the time expense needed for SPECT image processing are scarce. However, our results compare favourably with previously published data on automated alignment of images of rigid body parts, such as the brain (6, 19). The approach evaluated herein appears quite feasible and can easily be implemented into the routine clinical work flow.

Probably due to considerable variability of tracer uptake in single lesions, no significant relationship between relative uptake values and the distance of the lesions to the

surface of the body could be demonstrated, even when ROI size was introduced as a covariate into the analysis. Whereas more centrally located lesions were depicted with higher contrast to background, apparent tracer uptake decreased in foci located within roughly 8 cm of the surface of the body (26) . As already shown in phantom studies, the lesion detectability was approximately linearly correlated with the depth of the lesion (Fig. 3). Furthermore, the visualization of liver uptake was more homogeneous on the attenuation-corrected images. This finding was confirmed by an additional phantom study. These results clearly demonstrate the effectiveness of the approach to attenuation correction studied herein.

Up to now, the effect of attenuation correction was evaluated mainly in cardiac SPECT imaging using data generated by line sources mounted on the gantry ring. There are several reports about improved image quality by reduction of the attenuation artefacts in the inferior myocardial wall which is particularly predisposed to attenuation artefacts. Prvulovich et al. (20) used gadolinium-153 line sources and found improved homogeneity of myocardial thallium-201 distribution. In this study, attenuation correction significantly diminished the dependence of tracer distribution on patient size, shape and density. Their findings were confirmed by multiple other investigators using a similar approach (3).

More recently, Kashiwagi et al. performed attenuation correction of cardiac SPECT images using separately acquired high performance CT (12) and observed a minimization of the artificial activity reduction in the inferior myocardial wall as well as reduction in lung activity. The latter data were also reported by Gustafsson et al. in an identical setup (7). However, in contrast to our study, these two groups placed the CT and the gamma camera next to each other, used identical flat patient tables, and attached fiducial markers to the skin enabling automatic image fusion. In summary, the real clinical usefulness of attenuation-correction for myocardial SPECT is still on debate (4).

A few years ago, a combined SPECT/CT imaging device consisting of a gamma camera with an integrated X-ray tube for combined transmission and emission tomography was introduced and several papers report a benefit of anatomico-functional image fusion on the diagnostic interpretation of SPECT (14, 18). These reports also address the detectability of tumour lesions in somatostatin receptor scintigraphy. However, none of these studies systematically evaluated the effect of attenuation correction on their data, although this can easily be performed when using this hybrid system.

In oncological PET with ^{18}F-deoxyglucose (FDG), attenuation correction is routinely performed. However, evidence on its effect on lesion contrast is scarce. Bengel et al. observed that the target to background contrast was higher in uncorrected images independent of the location of the lesions and their distance from the surface of the body (2). This discrepancy with our results may be explained by the additional noise from the transmission measurement in PET using transmission data obtained with ^{68}Ge rod sources, as already discussed by the authors. Another reason for the different findings may be the lack of scatter correction in the above mentioned data. Furthermore, Bai et al. reported in a very recent publication that images reconstructed by filtered backprojection, which was used by Bengel, and iterative reconstruction applied in our case, have very different appearances (1).

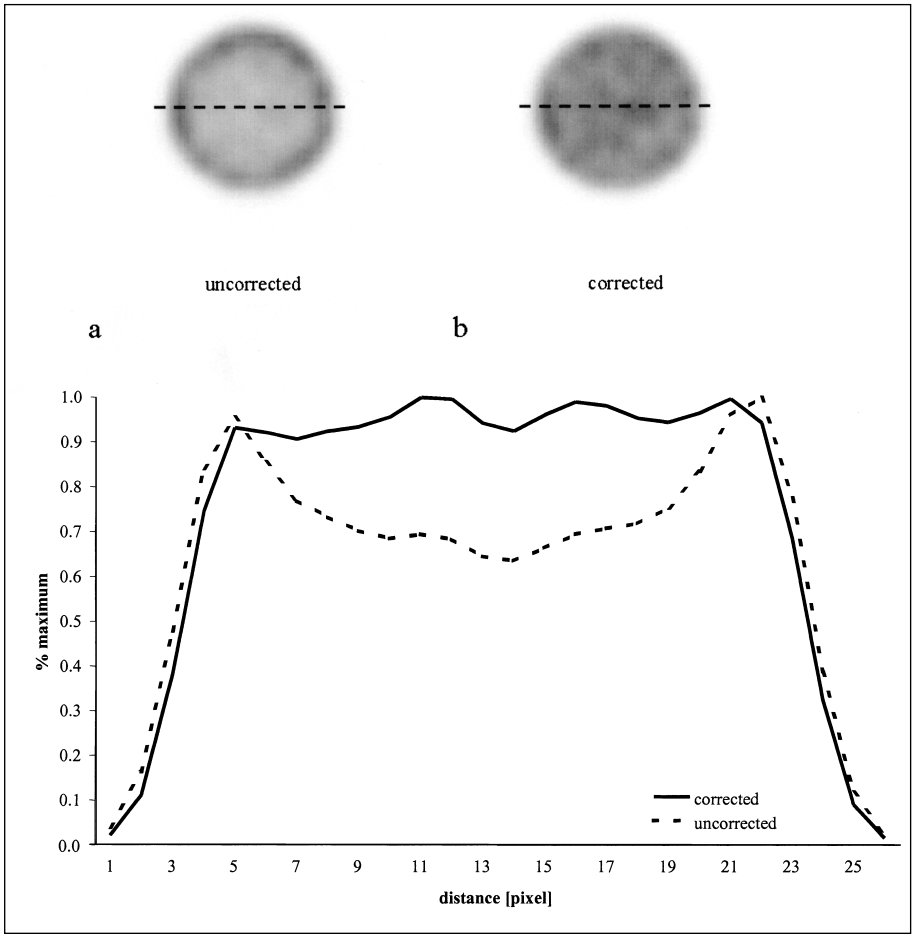

Fig. 5 Transaxial images from SPECT of a phantom filled with indium-111 without (a) and with (b) attenuation correction. Images show improved homogeneity of tracer distribution after attenuation correction. Curves (c) represent line profiles from right to left comparing attenuation-corrected and uncorrected slices. Note closely, reconstructing nuclear medicine data with a narrow beam attenuation map may cause an over-correction as raw data include scatter fraction. The crude method to correct this problem is to reduce attenuation values by some factor, which depends on the energy of the tracer and the acquisition window width. The implemented attenuation map activity allows entering corrective factors through the Broad Beam Coefficients. Therefore and as expected, the curve (c) shows a flat profile throughout the phantom.

It may be questioned whether the attenuation correction of SPECT images improves diagnostic accuracy. Our data do not lend themselves to answer this question due to the small number of patients studied. Theoretically, the increase in the contrast between uptake in more centrally located lesions and that in background should make their detection easier. However, the reduction in this parameter for lesions at a distance of less than 8 cm from the surface of the body would be a disadvantage, potentially precluding their discovery. A display of both the attenuation-corrected and the non-corrected data sets would maximize diagnostic accuracy.

Limitations

The major drawback of attenuation correction performed using separately acquired CT data is the difficulty to exactly match SPECT and CT data sets depicting non rigid body parts. In particular, differences in breath mode, shape of bed, and position of the patient limit the accuracy of alignment between two studies performed separately from each other (13). Several mathematical approaches have been developed to correct for these differences and to match image data from different modalities in an automated fashion (10). To date, all of these approaches perform less than satisfactorily (9), so that the interactive alignment of data from two different imaging modalities currently seems the best method. However, its accuracy resides in the judgement of the physician processing the images and can be proven accurate in individual patients only with considerable difficulty. Again, since image registration was performed by visual alignment of the SPECT and CT images using internal landmarks such as the contours of the body, of the liver and of organs exhibiting intensive tracer uptake such as the spleen, the kidneys, or neoplastic lesions, no noticeable artefacts from differences in breath mode could be detected.

Clearly, some of the problems mentioned can be overcome using hybrid systems or fiducial external markers (12). Nevertheless, a substantial number of CT studies will be performed without the awareness that fusion with SPECT will be required afterwards. Furthermore, from the point of view of radiation safety and cost effectiveness, the repetition of CT scanning for the sole purpose of obtaining data for attenuation correction is prohibited. Therefore, a compromise between the theoretically optimal process of attenuation correction and clinical feasibility has to be found. Our results indicate that the approach presented here is feasible and cost-effective method of acquiring this type of attenuation correction.

Conclusion

Attenuation correction of SPECT images performed by the use of separately acquired CT data is quick and simple. It improves the target to background contrast of lesions located more centrally in the body and homogenizes the visualisation of tracer uptake in the liver without additional radiation burden. These results suggest that investigations should be carried out to determine if these findings translate into improvement of diagnostic accuracy.

Acknowledgements
The authors thank Siemens Medical Solutions for providing the software for attenuation correction used herein. They are indebted to the technologists of the Clinic of Nuclear Medicine for technical support. Dr. Carsten Hocke's assistance with the phantom studies is also gratefully acknowledged. We appreciate Prof. Frank S. Torok's review of the manuscript.

References

1. Bai C, Kinahan PE, Brasse D et al. An analytic study of the effects of attenuation on tumor detection in whole-body PET oncology imaging. J Nucl Med 2003; 44: 1855-61.
2. Bengel FM, Ziegler SI, Avril N et al. Whole-body positron emission tomography in clinical oncology: comparison between attenuation-corrected and uncorrected images. Eur J Nucl Med 1997; 24: 1091-8.
3. Corbett JR, Ficaro EP. Attenuation corrected cardiac perfusion SPECT. Curr Opin Cardiol 2000; 15: 330-6.
4. Corbett JR, Kritzman JN, Ficaro EP. Attenuation correction for single photon emission computed tomography myocardial perfusion imaging. Curr Cardiol Rep 2004; 6: 32-40.
5. Ficaro EP. Should SPECT attenuation correction be more widely employed in routine clinical practice? For. Eur J Nucl Med Mol Imaging 2002; 29: 409-12.
6. Fiedler E, Platsch G, Schwarz A et al. Time consumption and quality of an automated fusion tool for SPECT and MRI images of the brain. Nuklearmedizin 2003; 42: 215-9.
7. Gustafsson A, Jacobsson L, Johansson A et al. Evaluation of various attenuation corrections in lung SPECT in healthy subjects. Nucl Med Commun 2003; 24: 1087-95.
8. Hubbell JH, Berger MJ. In: Jaeger RG (ed). Engineering Compendium on Radiation Shielding (IAEA, Vienna). Vol. 1, Ch. 4: 167-202. Berlin: Springer 1968.
9. Hutton BF, Braun M, Thurfjell L et al. Image registration: an essential tool for nuclear medicine. Eur J Nucl Med Mol Imaging 2002; 29: 559-77.
10. Hutton BF, Braun M. Software for image registration: algorithms, accuracy, efficacy. Semin Nucl Med 2003; 33: 180-92.
11. Kaczirek K, Prager G, Kienast O et al. Combined transmission and ^{99m}Tc-sestamibi emission tomography for localization of mediastinal parathyroid glands. Nuklearmedizin 2003; 42: 220-3.
12. Kashiwagi T, Yutani K, Fukuchi M et al. Correction of nonuniform attenuation and image fusion in SPECT imaging by means of separate X-ray CT. Ann Nucl Med 2002; 16: 255-61.
13. Keidar Z, Israel O, Krausz Y. SPECT/CT in tumor imaging: technical aspects and clinical applications. Semin Nucl Med 2003; 33: 205-18.
14. Krausz Y, Keidar Z, Kogan I et al. SPECT/CT hybrid imaging with ^{111}In-pentetreotide in assessment of neuroendocrine tumours. Clin Endocrinol (Oxf) 2003; 59: 565-73.
15. Kuwert T, Morgenroth C, Woesler B et al. Influence of size of regions of interest on the measurement of uptake of 123I-alpha-methyl tyrosine by brain tumours. Nucl Med Commun 1996; 17: 609-15.
16. Matsunari I, Boning G, Ziegler SI et al. Effects of misalignment between transmission and emission scans on attenuation-corrected cardiac SPECT. J Nucl Med 1998; 39: 411-6.
17. O'Connor M K, Kemp B, Anstett F et al. A multicenter evaluation of commercial attenuation compensation techniques in cardiac SPECT using phantom models. J Nucl Cardiol 2002; 9: 361-76.
18. Pfannenberg AC, Eschmann SM, Horger M et al. Benefit of anatomical-functional image fusion in the diagnostic work-up of neuroendocrine neoplasms. Eur J Nucl Med Mol Imaging 2003; 30: 835-43.
19. Pfluger T, Vollmar C, Wismüller A et al. Quantitative comparison of automatic and interactive methods for MRI-SPECT image registration of the brain based on 3-dimensional calculation of error. J Nucl Med 2000; 41: 1823-9.
20. Prvulovich EM, Lonn AH, Bomanji JB et al. Effect of attenuation correction on myocardial thallium-201 distribution in patients with a low likelihood of coronary artery disease. Eur J Nucl Med 1997; 24: 266-75.

21. Townsend DW, Beyer T, Blodgett TM. PET/CT scanners: a hardware approach to image fusion. Semin Nucl Med 2003; 33: 193-204.
22. Turkington TG, Gilland DR. CT-based attenuation correction for SPECT. In: von Schulthess GK (ed). Clinical molecular anatomic imgaing: PET, PET/CT, and SPECT/CT. Philadelphia: Lippincott Williams & Wilkins 2003: 59-63.
23. Vija AH, Hawman EG, Engdahl JC. Analysis of SPECT OSEM reconstruction method with 3D beam modelling and optional attenuation correction: Phantom studies. 2003 IEEE Nuclear Science Symposium, Medical Imaging Conference, Portland, USA, 19.-26.11.2003, Conference Record.
24. Wackers FJ. Should SPET attenuation correction be more widely employed in routine clinical practice? Against. Eur J Nucl Med Mol Imaging 2002; 29: 412-5.

Correspondence to:
Dr. Wolfgang Römer
Nuklearmedizinische Klinik
Universität Erlangen-Nürnberg
Krankenhausstr. 12
91054 Erlangen
Tel. +49-9131-853-3411
Fax. +49-9131-853-9262
E-Mail: wolfgang.roemer@nuklear.imed.uni-erlangen.de